Regular Article

PHYSICAL CHEMISTRY RESEARCH
Published by the
Iranian Chemical Society
www.physchemres.org
info@physchemres.org

Phys. Chem. Res., Vol. 12, No. 4, 1111-1131, December 2024
DOI: 10.22036/pcr.2024.466280.2548

Fabrication and Characterization of Nanoporous Ag/ZnO/SBA-16: Its Applications as Drug Delivery Systems

M.H. Fekri*, M. Razavimehr, S. Soleymani and F. Saki

Department of Chemistry, Faculty of Basic Sciences, Ayatollah Boroujerdi University, Boroujerd, Iran

(Received 4 July 2024, Accepted 13 September 2024)

In this research, the Ag/ZnO/SBA-16 was synthesized and used as loading and release of phenobarbital drug. To identify and characterize the properties of Ag/ZnO/SBA-16 nanostructure, several identification methods such as XRD, FTIR, BET, EDX, SEM, and TEM were used. The influence of various parameters was investigated using the RSM methodology, by experimental design (DOE) software. Drug release in three different environments at 37 °C including aqueous, acidic, and alkaline was studied. The isotherm and kinetic studies showed that the drug loading process follows the Freundlich isotherm and the Higuchi kinetics model. The thermodynamic study also showed that drug loading on Ag/ZnO/SBA-16 nanocomposite is an exothermic and spontaneous process at low temperatures.

Keywords: Composite, Phenobarbital, Drug release, Design of experiment, Isotherm, Spontaneous process

INTRODUCTION

The science of nanotechnology is very promising in the pharmaceutical industry. Because by using new drug targeting systems, drugs are produced that are much more effective and bring more profit. These effects become more obvious when we know that currently, 13% of the huge pharmaceutical industry market is related to the sale of products including silicate drug delivery systems [1]. Designing and manufacturing controlled drug release systems can be very useful in managing treatment methods by drugs. So far, many materials have been introduced as drug release systems, among which we can mention biodegradable polymer materials, ceramic materials such as hydroxyapatite, calcium phosphates, SBA family, *etc*. [2-4]. With the controlled and targeted drug delivery method, the toxicity of the drug, its destruction, and its repeated use are prevented. Biocompatibility and drug loading capacity are important characteristics that are considered for materials needed as drug carriers. The design of these materials must be done properly to prevent rapid diffusion. Therefore, mesoporous materials are used as drug carriers due to their unique properties such as higher surface-to-volume ratio, controllable particle size effect, as well as biocompatibility and biodegradability. Today, research on mesoporous silica nanoparticles for medical purposes has increased [5-8]. In fact, the high porosity of mesoporous silica materials allows biologically active molecules of different sizes to settle in the cavities of these materials [9]. Also, the regular porosity network of these materials makes it possible to achieve a suitable loading and releasing speed. On the other hand, since the adsorption of molecules in mesoporous materials is a surface phenomenon, the specific surface of these materials also leads to the adsorption of more biologically active molecules [10].

From the beginning of the 21st century, attempts to make various types of silica nanoparticles began. By using organic silanes along with structure-directing agents or shapers and a mixture of water and alcohol as a solvent, new mineral substrates with regular structures in nanometer dimensions were prepared [11]. Silica-based mesoporous Santa Barbara amorphous (SBA) materials have been widely used as drug delivery systems. Among these materials, SBA-15 and SBA-16 were quickly noticed because they have desirable surface

*Corresponding author. E-mail: m.h.fekri@abru.ac.ir

and physicochemical properties such as low toxicity, biocompatibility, biodegradability, and synthesis using cheap materials. SBA-15 and SBA-16 are three-dimensional silicate porous materials including SiO_2 and surface hydroxyl (OH) groups, which are prepared using non-ionic copolymers as a template and have an amorphous structure like other porous materials [12]. SBA-15 crystallizes in a hexagonal structure, while SBA-16 has a cubic crystal structure. SBA-16 has attracted more attention due to its three-dimensional cubic structure with open channels according to the Im3m space group. SBA-16, the main subset of these materials, particles containing parallel open mesochannels with a narrow and tunable pore size distribution in a wide range from 2 to 50 nm, high surface area, uniform pore size, high pore volume, thermal and chemical stability, hydrophobicity or Controllable hydrophilicity, insolubility in water, non-toxic, significant mechanical resistance and high concentration of active sites on their surfaces, biocompatible and biodegradable, wall thickness of about 3 to 4 nm, and have higher mechanical stability and hydrothermal stability than MCM-41 compounds [13]. These properties make these materials dominant for absorption, so nanoparticles can easily disperse evenly among these holes and improve the resulting mesoporous properties. On the other hand, by loading nanoparticles on SBA, its aggregation is prevented. In addition, it makes the nanocarrier more effective as a drug delivery system [14]. However, these mesoparticles do not have a wide range of functional groups on their surfaces (mainly containing silane groups), which limits the possible applications of these materials for specific target molecules. As a solution, many studies have made modifications to the active sites of SBA-16, adding a variety of ligands (organic groups, coordination compounds, nanoparticles, metal oxides, etc.) and loading different compounds onto them. have provided [15,16].

ZnO NPs are one of the most widely used metal oxide NPs in a variety of sectors and research institutions since they possess significant applications [17]. Because of the small particle size of nano-ZnO, the human body can easily absorb zinc. Since ZnO NPs are relatively affordable and less toxic than other metal oxide NPs, they offer a wide range of other medicinal uses, including antimicrobial, anti-diabetic, anti-inflammatory, anti-aging, and also in wound healing and bio-imaging [18-21]. ZnO NPs have a high biocompatibility, allowing them to be used in a therapeutic environment for antibacterial, antifungal, antiviral, and anticancer properties [22]. Several types of inorganic metal oxides, such as TiO_2, CuO, and ZnO have been produced and have remained in current investigations, but ZnO NPs are the most interesting of these metal oxides since they are inexpensive to make, safe, and simple to prepare [23]. Furthermore, the following characteristics must be present in any agent intended for human consumption for treating various diseases. It should be nontoxic, must not react with food or the container, should have a pleasant flavor or be tasteless, and should not have an unpleasant odor. ZnO NPs are one such inorganic metal oxide that meets all of the aforementioned criteria, allowing them to be used safely as a medication, package preservative, and antibacterial agent [24,25]. Hence, the US Food and Drug Administration (FDA) has classified ZnO NPs as a "GRAS" (generally regarded as safe) substance [26]. Silver nanoparticles (Ag NPs), on the other hand, possess anticoagulant and anti-inflammatory activity, which makes them ideal candidates for biological applications [27].

Phenobarbital (Fig. 1) was marketed in 1912 by the pharmaceutical company Bayer under the brand name Luminal. Until the introduction of benzodiazepines in the 1960s, this drug remained only a common sedative and hypnotic. Phenobarbital is a barbiturate drug. This drug is usually used to treat epilepsy and seizures in young children [28].

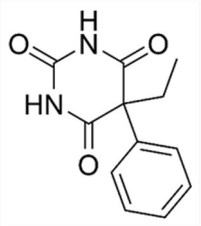

Fig. 1. Structure of PHB drug.

In this research, due to the simple synthesis process and well-defined morphology, large pore size, and especially the three-dimensional connection of the pores that lead to better mass transfer, Ag/ZnO/SBA-16 mesoporous were used as phenobarbital drug carriers. The newly synthesized nanocomposite was used after identification by different techniques (XRD, SEM, TEM, *etc*.) to investigate drug loading and release studies. In this work, with the help of

experiment design software, the optimal conditions of drug loading on nanocomposite were obtained. 5 effective variables in drug loading including pH, contact time, temperature, drug concentration, and amount of nanocomposite were considered. Then, the release of the drug was studied in three neutral, acidic, and alkaline environments.

EXPERIMENTAL

Pluronic copolymer f127 was obtained from Sigma Aldrich. This substance was used as a surfactant for the synthesis of SBA-16. The chemical formula of this substance is $(C_3H_6O.C_2H_4O)_x$. For the synthesis of SBA-16, tetraethyl orthosilicate (TEOS) solution with a molecular formula $Si\,C_8H_{20}O_4$ was used as a source of silica. TEOS was obtained from Sigma Aldrich Co. with a molecular weight of 208.3 g mol^{-1} and a density of 0.933 g ml^{-1}. NaH_2PO_4 and Na_2HPO_4 (Merck Co.) salts were used to prepare buffer solutions. A dialysis bag with an average flat width of 23 mm (14000MWCO, 99.99% retention) was used to release the drug (Sigma Aldrich Company). $AgNO_3$, HCl, and 1-butanol were obtained from Merck. Phenobarbital drug with formula $C_{12}H_{12}N_2O_3$ and molecular weight 232.235 g mol^{-1} was obtained from Iran Food and Drug Organization.

First, 1.5 g of pluronic copolymer f127 was added to a 250 ml Erlenmeyer flask and dissolved in 72 ml of distilled water. Then 7.2 ml of concentrated hydrochloric acid was added to it, the solution was stirred for 30 min at 60 °C. Then, 7.7 ml of tetraethyl orthosilicate and 5.5 ml of 1-butanol were added to the solution. Again, the solution was placed on a magnetic stirrer at a temperature of 55 °C for 24 h. After this time, the solution was placed in an oven with a temperature of 100 °C for 24 h. To perform calcination on the prepared precipitate, it was first washed and then placed in an oven with a temperature of 600 °C for 24 h. Finally, the white powder of SBA-16 was synthesized [29].

89.9 g of $ZnSO_4.7H_2O$ and 25 g of NaOH were dissolved in 250 ml of distilled water to form solutions with certain concentrations, respectively. The two solutions were added dropwise under vigorous stirring for 12 h at 65 °C. ZnO nanoparticles (ZnO NPs) samples were filtered and collected by centrifugation and washed with pure ethanol [30].

In this work, zinc oxide and SBA-16 were chosen with a ratio of 1:5. Then, each of them was placed in ultrasonic for 30 min. Then, the two solutions were mixed together and placed on a magnetic stirrer for 24 h at 30 °C. In the end, it was placed in an oven at 80 °C for 24 h to dry the sample [31].

0.4 g of ZnO/SBA-16 was added to 10 ml of 0.1 M $AgNO_3$ and stirred for 6 h in the absence of light. Then it was placed in the oven at a temperature of 70 °C for 12 h [32].

To load the phenobarbital drug, solutions with concentrations of 10, 20, 30, 40, and 50 ppm were prepared from the PHB drug. Then 50 ml of each of these solutions were mixed with specific amounts of Ag/ZnO/SBA-16 nanocarrier (0.01, 0.02, 0.03, 0.04, and 0.05 g) and 15 min were placed in the ultrasonic and then were stirred by a magnetic stirrer for 3 h. The absorbance of solutions was read by UV-Vis spectrophotometer. The amount of drug loading was obtained from Eq. (1):

$$EE\% = \frac{(C_0 - C_e)}{C_0} \times 100 \qquad (1)$$

Where C_0 and C_e are the initial and residual concentrations of the drug, respectively.

To draw the calibration curve (Fig. 2), a stock solution with a concentration of 1000mg/liter was prepared from the drug phenobarbital. Then concentrations of 20 to 100 ppm were prepared using the stock solution and their absorbance was read as λ_{max} = 276.

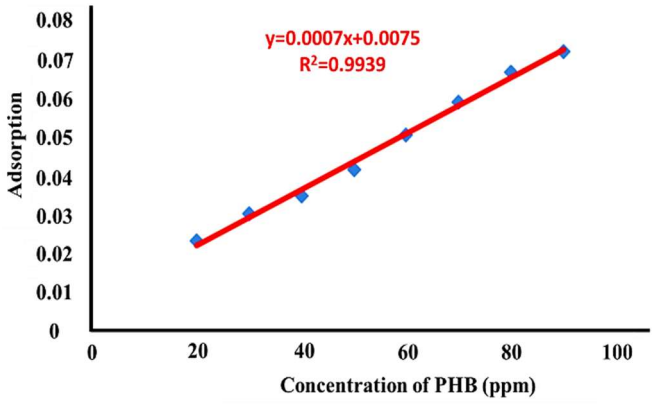

Fig. 2. Calibration curve of PHB drug.

At zero point charge (pH_{PZC}), the positive and negative charges are equal, so at this point, the surface charge is zero [33]. To obtain the pH_{PZC}, 0.01 g of the PHB Drug was dissolved in 15 ml of distilled water and the pH of the solution was set in the range of 2-12 as the initial pH. Then it was placed on a magnetic stirrer for 1 h. After this, the final pH was read. According to Fig. 3, pH_{PZC} was obtained at 7.9. If there was no surface charge, the graph would be red, but due to the surface charge, the pH value would be different and the actual graph would be green.

Experiments always cost money and time. Therefore, the goal of every engineer or researcher is to conduct effective experiments that obtain the most information with the least cost and time, and with the increase in the number of factors, this cost and time increases. Therefore, there is a need for a method that can obtain the most information about the process with the least cost and time, provide logical conclusions, and obtain documentary evidence about the process. The design of the experiment method is a statistical method that is used in the development of statistical models to solve various equations [34]. This method is based on predicting the functional relationship between the response and the experimental variables. It also optimizes variables. The design of the experiment method uses a series of designed experiments and obtains the optimal response for the entire method, which depends on the process variables. On the other hand, by using the response level method, in addition to investigating the influence of independent parameters on the response, the mutual influence of independent parameters on the response, which is the percentage of drug loading, can be investigated [35,36]. In drug delivery processes, it is important to optimize effective parameters to achieve maximum drug loading on the drug carrier. In this work, the absorption percentage of phenobarbital drug by Ag/ZnO/SBA-16 nanocarrier was chosen as the final answer for the design of the experiment, and the statistical method of using several variables was investigated in order to optimize the conditions. Therefore, with the help of experimental design, 5 important variables in drug loading including pH, initial concentration of the drug, amount of drug carrier, temperature, and contact time were considered in 5 levels (Table 1). The results were fitted using Eq. (2).

$$Y = \beta_0 + \sum_{i=1}^{5} \beta_i X_i + \sum \beta_{ij} X_i X_j \quad (2)$$

Where X_i and X_j are independent variables, Y is the dependent variable or response, and β is the fitting coefficient. In this research, 50 tests were suggested by the software (Table 2).

pH_i	2.00	3.00	4.00	5.00	6.00	7.00	8.00	9.00	10.00	11.00	12.00
pH_f	2.11	6.67	6.70	6.75	6.83	7.25	7.95	8.46	9.76	10.97	11.96

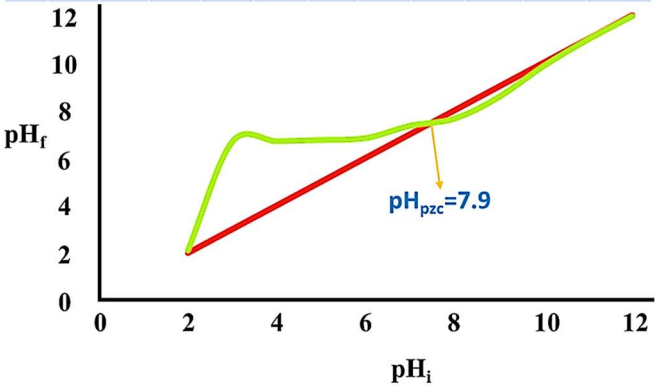

Fig. 3. pH_{PZC} of PHB drug.

Table 1. Effective Factors of Drug Loading by Ag/ZnO/SBA-16 Nanocarrier by CCD Design

Parameter	Component	Unit	Applied level				
			(-2)	(-1)	(0)	(+1)	(+2)
A	pH	-	2	4	6	8	10
B	NCD	g	0.01	0.02	0.03	0.04	0.05
C	ICT	ppm	10	20	30	40	50
D	Temp.	°C	30	40	50	60	70
E	CT	min	10	20	30	40	50

Table 2. Proposed Software Tests and Experimental Results at Low, Center, and High Levels

Std	Run	Factor 1 A: pH	Factor 2 B: comp. dose	Factor 3 C: cons. drug	Factor 4 D: temp.	Factor 5 E: cont. time	Response 1 load
		-	g	ppm	C	min	%
34	1	10.00	0.03	30.00	50.00	30.00	46.00
13	2	4.00	0.02	40.00	60.00	20.00	79.25
37	3	6.00	0.03	10.00	50.00	30.00	80.50
20	4	8.00	0.04	20.00	40.00	40.00	67.75
2	5	8.00	0.02	20.00	40.00	20.00	61.50
36	6	6.00	0.05	30.00	50.00	30.00	88.50
8	7	8.00	0.04	40.00	40.00	20.00	62.00
46	8	6.00	0.03	30.00	50.00	30.00	80.25
4	9	8.00	0.04	20.00	40.00	20.00	66.50
14	10	8.00	0.02	40.00	60.00	20.00	58.00
5	11	4.00	0.02	40.00	40.00	20.00	89.75
38	12	6.00	0.03	50.00	50.00	30.00	73.50
26	13	8.00	0.02	20.00	60.00	40.00	57.10
33	14	2.00	0.03	30.00	50.00	30.00	99.50
48	15	6.00	0.03	30.00	50.00	30.00	80.50
27	16	4.00	0.04	20.00	60.00	40.00	99.50
44	17	6.00	0.03	30.00	50.00	30.00	80.25
19	18	4.00	0.04	20.00	40.00	40.00	100
43	19	6.00	0.03	30.00	50.00	30.00	80.50
9	20	4.00	0.02	20.00	60.00	20.00	85.00
11	21	4.00	0.04	20.00	60.00	20.00	94.00
1	22	4.00	0.02	20.00	40.00	20.00	90.50
21	23	4.00	0.02	40.00	40.00	40.00	90.25
39	24	6.00	0.03	30.00	30.00	30.00	77.50
22	25	8.00	0.02	40.00	40.00	40.00	66.00
41	26	6.00	0.03	30.00	50.00	10.00	73.50
30	27	8.00	0.02	40.00	60.00	40.00	61.00
3	28	4.00	0.04	20.00	40.00	20.00	98.00
12	29	8.00	0.04	20.00	60.00	20.00	64.25
45	30	6.00	0.03	30.00	50.00	30.00	80.50
6	31	8.00	0.02	40.00	40.00	20.00	66.50
29	32	4.00	0.02	40.00	60.00	40.00	83.00
49	33	6.00	0.03	30.00	50.00	30.00	80.00
28	34	8.00	0.04	20.00	60.00	40.00	68.50
10	35	8.00	0.02	20.00	60.00	20.00	57.50
17	36	4.00	0.02	20.00	40.00	40.00	88.00
31	37	4.00	0.04	40.00	60.00	40.00	87.00
15	38	4.00	0.04	40.00	60.00	20.00	79.00
18	39	8.00	0.02	20.00	40.00	40.00	58.50
25	40	4.00	0.02	20.00	60.00	40.00	86.20
47	41	6.00	0.03	30.00	50.00	30.00	80.50
42	42	6.00	0.03	30.00	50.00	50.00	78.00
40	43	6.00	0.03	30.00	70.00	30.00	68.50
50	44	6.00	0.03	30.00	50.00	30.00	79.75
23	45	4.00	0.04	40.00	40.00	40.00	91.50
32	46	8.00	0.04	40.00	60.00	40.00	62.50
35	47	6.00	0.01	30.00	50.00	30.00	79.75
24	48	8.00	0.04	40.00	40.00	40.00	66.00
7	49	4.00	0.04	40.00	40.00	20.00	87.00
16	50	8.00	0.04	40.00	60.00	20.00	56.00

Drug release was performed using a dialysis bag in three neutral, acidic, and alkaline environments as an external solution or simulated body environment. The neutral medium was distilled water with pH = 6.8 and the acidic and alkaline mediums were buffer solutions with pH 4.8 and 7.4, respectively. A solution of 500 ml was prepared from each of the external environments. Then the dialysis bag containing the drug solution and nanocarrier was transferred inside them. This set was placed on a magnetic stirrer. Drug release experiments were tested at 1, 2, 3, 4, 12, 24, 48, 72, and 96 h.

RESULTS AND DISCUSSION

According to the FTIR analysis of nano silicate SBA-16, a broad peak in the range of 3441.12 cm^{-1} associated with the symmetric stretching vibration of the O-H bond is observed, which is the result of silanol groups. Also, the observed peak in the area of 1630.95 cm^{-1} is related to the stretching and bending vibrations of water molecules absorbed on the surface of SBA-16. The peaks at 462.52, 805.20, and 1086.21 cm^{-1} are related to the bending, symmetric, and asymmetric stretching vibrations of Si-O-Si, respectively [37]. A comparison of FTIR analysis from SBA-16 and ZnO/SBA-16 samples shows that the peak in the range of 463 cm^{-1} has become wider, while the intensity of the peak located at 805 cm^{-1} has been weakened, which proved that ZnO has some interactions at the surface of mesoporous silica [8]. The FTIR spectra of SBA-16 and ZnO/SBA-16 samples are very similar to Ag/ZnO/SBA-16 silica nanocomposites, which provides good evidence for the physical interaction between Ag nanoparticles and the silica network. Also, according to the studies, the incorporation of metal into the silica framework causes changes in the intensity of the band located at 805 cm and is assigned to the stretching vibration of the Si-O-Me bond. Therefore, it is reasonable to suggest that silver is incorporated into the mesoporous silica framework in the Ag/ZnO/SBA-16 nanocomposite [38,39].

In the XRD spectrum, a strong peak at 2θ = 24° was observed for SBA-16, which corresponds to the reflection of the d100 crystal plane and indicates a cubic structure with an Im3m space group. This peak is the main indicator to identify SBA-16 [40]. The XRD pattern of ZnO/SBA-16 nanocomposite shows a peak at 2θ = 24° with low intensity. Also, seven peaks with intensity (110), (102), (101), (002), (100), (103), and (112) in the diffraction pattern of ZnO nanoparticles indicate the hexagonal wurtzite structure [41]. The XRD pattern of Ag/ZnO/SBA-16 in Fig. 5 shows that the structure of SBA-16 does not change significantly after Ag loading. However, the (110) characteristic peak is shifted 2 degrees lower after Ag loading, as well as the 2θ peak at 38.14° and 64.42° for metallic Ag (JCPDS No. 040783) indicated that the Ag/ZnO/SBA-16 composite had been prepared [42].

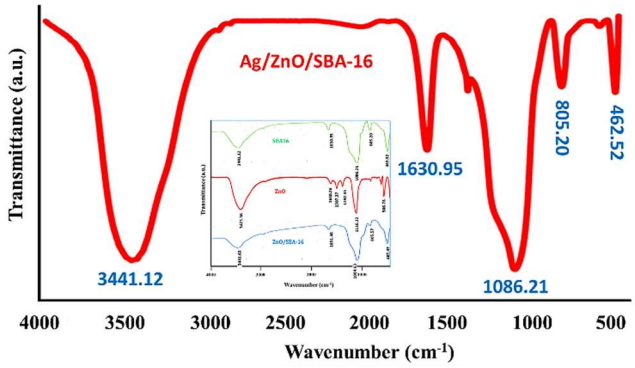

Fig. 4. FTIR spectra of Ag/ZnO/SBA-16.

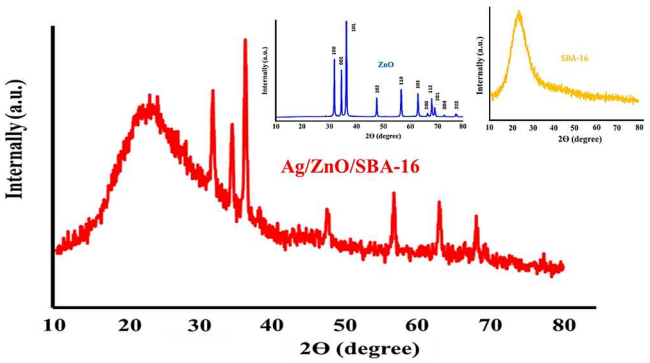

Fig. 5. XRD patterns of SBA-16, and ZnO/SBA-16 and Ag/ZnO/SBA-16.

According to the scanning electron microscope image (SEM) in Fig. 6, we can conclude that the morphology of SBA-16 after the placement of ZnO and Ag is spherical and there is no fundamental change in its structure. Figures 6c and 6d show the transmission electron microscope image of

Ag/ZnO/SBA-16 nanocomposite with 100 nm magnification. Black halos in the image indicate the presence of ZnO [43]. As can be seen in the figure, zinc oxide is completely uniformly distributed on the surface of SBA-16 mesostructure, which confirms that the Ag/ZnO/SBA-16 nanocomposite has been successfully synthesized. Moreover, many highly dispersed Ag nanoparticles are observed in the Cubic channels of SBA-16. The fringes in Fig. 6d give a d-spacing of 0.23 nm, corresponding to the (111) atomic planes of the cubic silver lattices [44].

EDX analysis of the mesostructure of SBA-16 (Fig. 7a) shows that silicon has the highest peak compared to other elements, which confirms that SBA-16 is a silicate material. The presence of Zn and Ag peaks in Fig. 7b confirms that the Ag/ZnO/SBA-16 nanocomposite has been correctly synthesized. It can also be seen that the peak related to Si is still the highest peak, which shows that in addition to the correct structure of the synthesized nanocomposite, this mesopore has maintained its silicate structure.

Figures 8a and 8b show the adsorption/desorption isotherm and BJH curve of Ag/ZnO/SBA-16 nanocarrier, respectively. Figure 8a shows that this nanocomposite has a type IV (a) isotherm (IUPAC nomenclature of the isotherms) and the absorption/desorption process formed a hysteresis loop [45]. When a compound forms a hysteresis loop in its isotherm diagram, it can be said that the compound is 100% mesoporous. Also, by using the adsorption-desorption isotherm diagram and the formed hysteresis loop, the geometry of the holes can be recognized. According to the diagram, the hysteresis loop is of H1 type. Therefore, the holes have a cylindrical geometry [46,47].

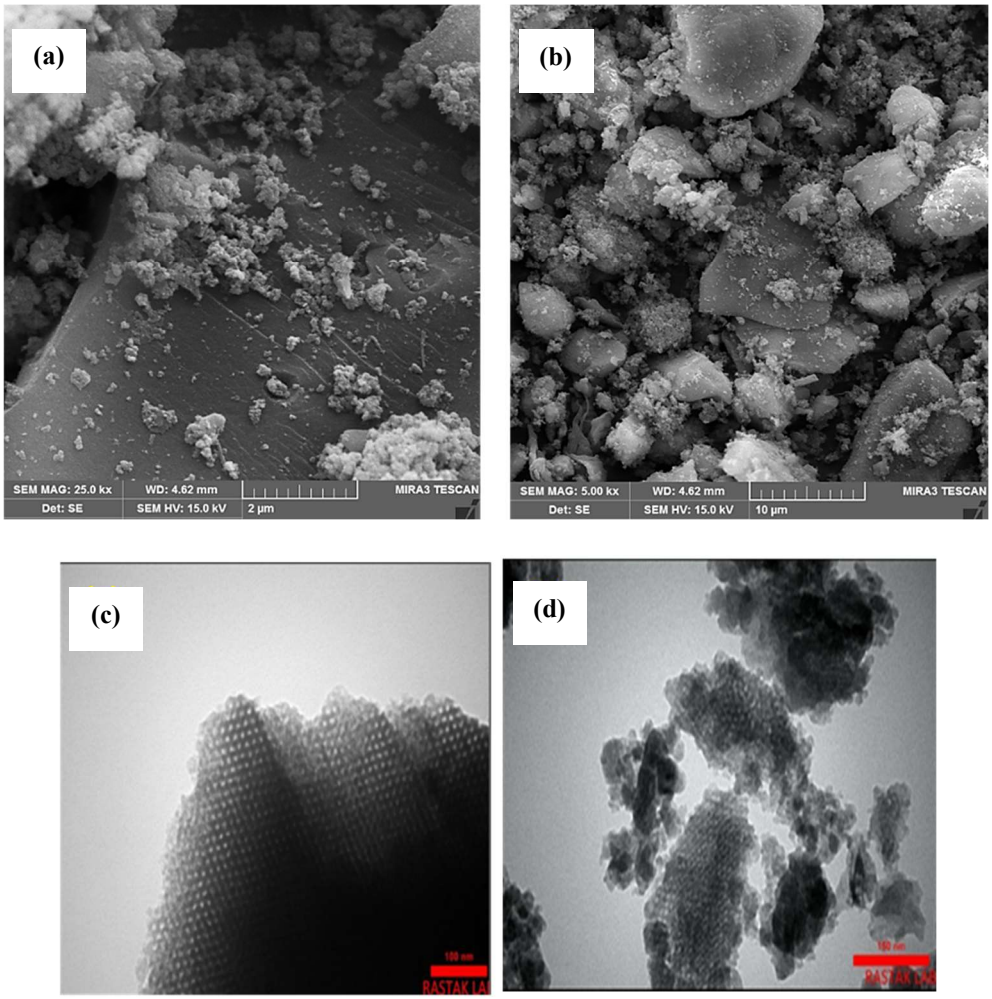

Fig. 6. Images of Ag/ZnO/SBA-16 nanocomposite (a,b) SEM analysis, (c,d) TEM analysis.

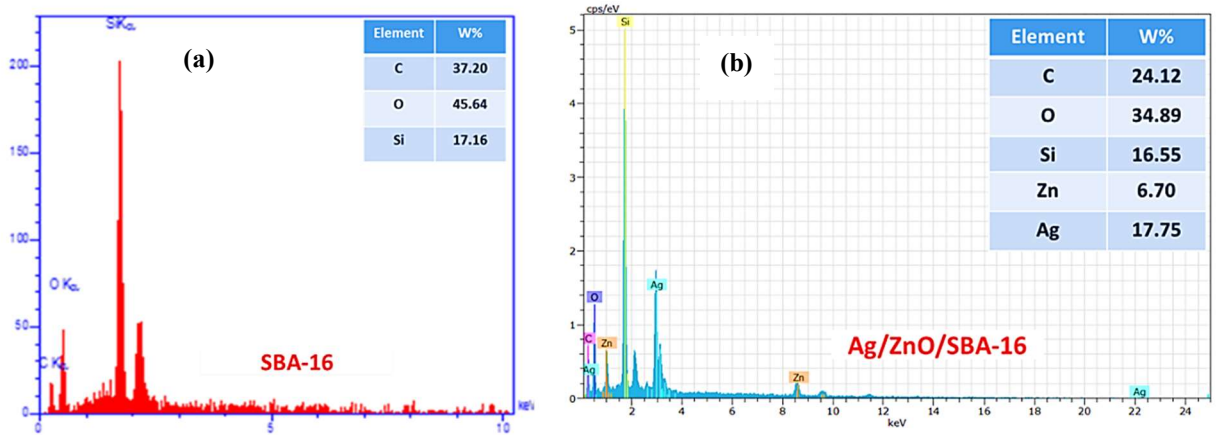

Fig. 7. EDX analysis of (a) SBA-16 and (b) Ag/ZnO/SBA-16.

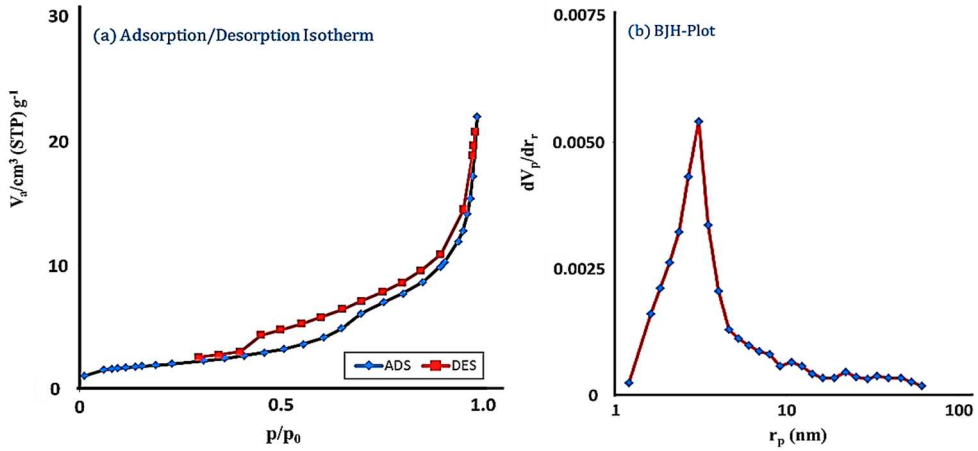

Fig. 8. (a)Adsorption/desorption analysis and (b) BJH-plot of Ag/ZnO/SBA-16 nanocomposite.

Figure 8b shows the BJH curve of the nanocomposite in the range of 1-100 nm. Using this curve, the size distribution of the holes can be measured. In the prepared nanocomposite, the maximum distribution of holes is in the range of 1-10 nm. Also, the BET analysis of Ag/ZnO/SBA-16 nanocomposite can be seen in Table 3. The results showed that the specific surface area of Ag/ZnO/SBA-16 nanocomposite is 276.87 $m^2 g^{-1}$. Also, the average particle diameter and pore volume were obtained as 10.90 nm and 0.5378 $cm^3 g^{-1}$, respectively. Therefore, it can be concluded that the synthesized nanocomposite is mesoporous. Based on a classification by IUPAC, materials whose pore sizes are between 2-50 nm are mesoporous, so nanoporous materials, which are a subset of nanostructured materials, have nanometer-scale pores [48]. This type of material with a very high internal surface area has a great ability to absorb and interact with atoms, molecules, and ions. According to the results obtained from BET analysis, it can be concluded that Ag/ZnO/SBA-16 is a nanostructure due to the presence of nano-scale holes.

Table 3. BET Analysis of Ag/ZnO/SBA-16 Nanocomposite

BET analysis	
V_m	61.74 [cm^3(STP) g^{-1}]
$a_{S, BET}$	276.87 [$m^2 g^{-1}$]
C	165. 60
Total pore volume ($p/p_0 = 0.986$)	0. 5378 [$cm^3 g^{-1}$]
Average pore diameter	10.90 [nm]

Table 4 shows the appropriate statistical model for drug loading on the adsorbent. The p-value and the regression coefficient are statistical parameters that are checked to measure the accuracy and correctness of the suitable model. If the p-value is less than 0.05 and the regression coefficient (R^2) is closer to 1, the model is more suitable [49]. As can be seen in Table 4, the quadratic model has a p-value less than 0.05 and the highest regression coefficient (0.9996) compared to the other 3 models.

Considering the Quadratic model, the statistical parameters obtained from the analysis of variance (ANOVA) are shown in Table 5. As can be seen, all parameters have p-values less than 0.05, which indicates the correct relationship between factors and parameters [50].

Table 4. Suitable Model Based on Statistical Analysis of Experimental Data

Source	Sequential p-value	Lack of fit p-value	Adjusted R^2	Predicted R^2	
Linear	< 0.0001	< 0.0001	0.9084	0.8930	
2FI	0.0004	< 0.0001	0.9492	0.9516	
Quadratic	< 0.0001	0.6069	0.9996	0.9992	Suggested
Cubic	0.8251	0.3602	0.9995	0.9929	Aliased

Table 5. Results of Analysis of Variance (ANOVA) for the Regression Models

Source	Sum of squares	df	Mean square	F-value	p-value	
Model	8442.86	20	422.14	5750.28	< 0.0001	Significant
A-pH	7164.99	1	7164.99	97598.91	< 0.0001	
B-comp. dose	197.80	1	197.80	2694.39	< 0.0001	
C-cons. drug	129.78	1	129.78	1767.82	< 0.0001	
D-temp.	202.28	1	202.28	2755.32	< 0.0001	
E-cont. time	55.34	1	55.34	753.86	< 0.0001	
AB	8.66	1	8.66	118.01	< 0.0001	
AC	80.80	1	80.80	1100.68	< 0.0001	
AD	4.61	1	4.61	62.84	< 0.0001	
AE	1.93	1	1.93	26.23	< 0.0001	
BC	185.04	1	185.04	2520.56	< 0.0001	
BD	7.95	1	7.95	108.29	< 0.0001	
BE	36.02	1	36.02	490.64	< 0.0001	
CD	37.30	1	37.30	508.13	< 0.0001	
CE	14.38	1	14.38	195.85	< 0.0001	
DE	20.40	1	20.40	277.88	< 0.0001	
A^2	106.91	1	106.91	1456.27	< 0.0001	
B^2	33.03	1	33.03	449.90	< 0.0001	
C^2	18.74	1	18.74	255.30	< 0.0001	
D^2	99.72	1	99.72	1358.38	< 0.0001	
E^2	37.17	1	37.17	506.37	< 0.0001	
Residual	2.13	29	0.0734			
Lack of fit	1.57	7	0.0716	0.9030	0.6069	Not significant
Pure error	0.5547	7	0.0792			
Cor total	8444.99	49				

Optimum values by graphic analysis and using Design Expert software can be extracted as surface curve (Fig. 9) and contour curve (Fig. 10) diagrams. These diagrams have the ability to check the simultaneous response of two variables. Contour diagrams represent the image of surface diagrams on the screen and are two-dimensional diagrams [51]. As the contour graph moves towards the red color, each factor provides a better level of response.

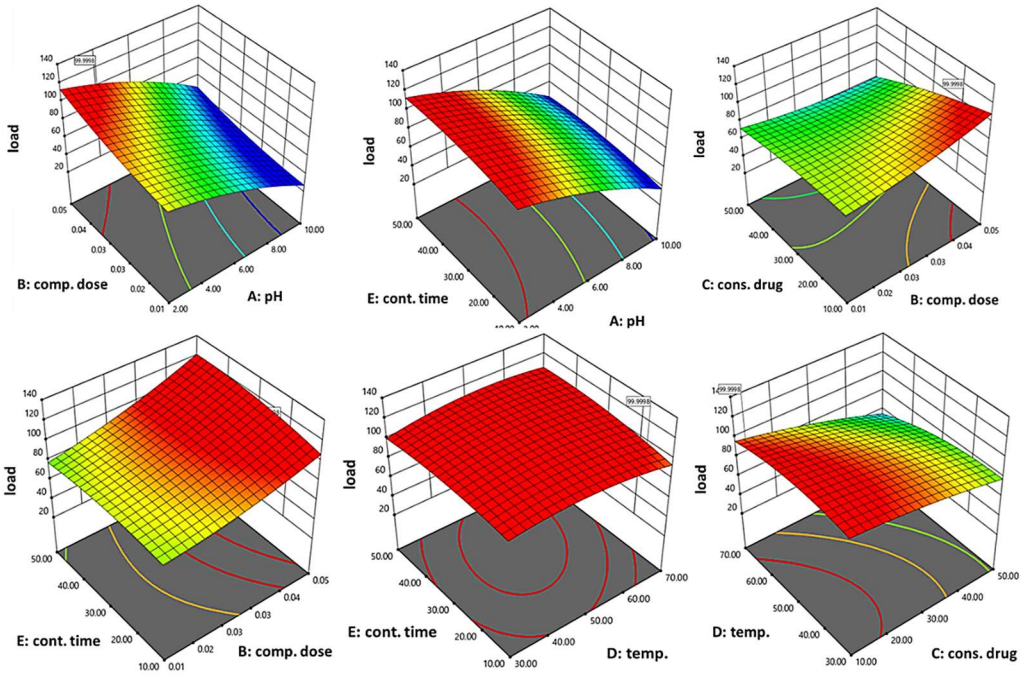

Fig. 9. Response surface diagrams for the effect of some factors on the resulting EE%.

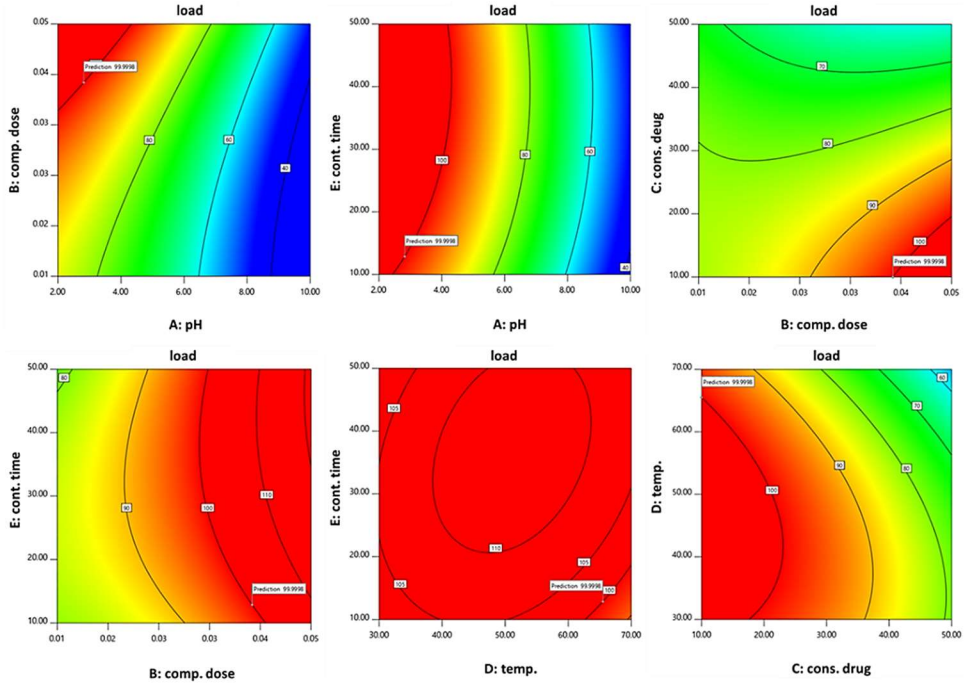

Fig. 10. Contour curves for the effect of some factors on the resulting EE%.

The normal probability curve shows how the residual values follow a normal distribution. Even though the data follows a normal distribution, some average distribution is expected. Therefore, the results show that the data have a normal distribution and are consistent with the model proposed by the software (Fig. 11a). The graph of actual values versus predicted values is shown in Fig. 8b. According to Fig. 11b, it can be seen that there is a good fit between these two values and the actual and predicted values are near to each other. The curve of standard residual values versus responses can be seen in Fig. 11c. This diagram shows the distribution of the results of the 50 proposed experiments by the experiment design software. According to the figure, all the results are within the confidence range of -4 to +4, which indicates a good fit between the model and the answers obtained [52,53]. The curve of the residual values versus the predicted values should have a random distribution. According to Fig. 11d, all the results are within the confidence range of -3 to +3. Also, the dispersion of the results can be seen. It is concluded that the model has the ability to describe the responses [54].

The coded equation related to the factors affecting the amount of drug loading is as follows:

$$\%Load = +80.24 - 13.38A + 2.22B - 1.80C - 2.25D + 1.18E - 0.5203AB + 1.59AC + 0.3797AD - 0.2453AE - 2.40BC + 0.4984BD + 1.06BE - 1.08CD + 0.6703CE + 0.7984DE - 1.83A^2 + 1.02B^2 - 0.7653C^2 - 1.77D^2 - 1.08E^2 \quad (3)$$

Five parameters significantly affected the load % of the drug onto the nanocomposite. The pH, composite dosage, initial concentration of the drug, the effect of temperature, and contact time factors were investigated by RSM method. The maximum amount of drug loading on Ag/ZnO/SBA-16 nanocomposite was observed at pH = 2.82 (Fig. 12a). The results showed that pH has an inverse relationship with loading percentage. At low pH (lower than pHpzc = 7.9), H^+ ions are placed on the nanocomposite sites and the nanocomposite surface becomes more positive. Therefore, the amine group of phenobarbital drug is protonated, and the drug loading rate increases. But at high pH (higher than pH_{pzc}), OH- ions increase on the surface of the nanocarrier and the repulsion between the surface and the drug reduces the amount of drug loading [55].

The effect of the dosage of Ag/ZnO/SBA-16 nanocomposite on the amount of EE% was investigated (Fig. 12b), which had a positive effect (p-value < 0.05). It was observed that the amount of drug loading increased with an increasing amount of nanocomposite. Because by increasing the amount of nanocarrier, a wide surface, and more active sites are available to the drug molecules, which results in more loading of the drug. The maximum amount of nanocomposite for drug loading is 0.04 g [56].

The initial drug concentration is also inversely proportional to the drug loading percentage (Fig. 12c). For the present study, the optimal initial drug concentration was 10 ppm. At higher concentrations, all the active sites of the drug carrier are occupied by drug molecules, as a result, the loading percentage decreases with the increase of the initial concentration [57].

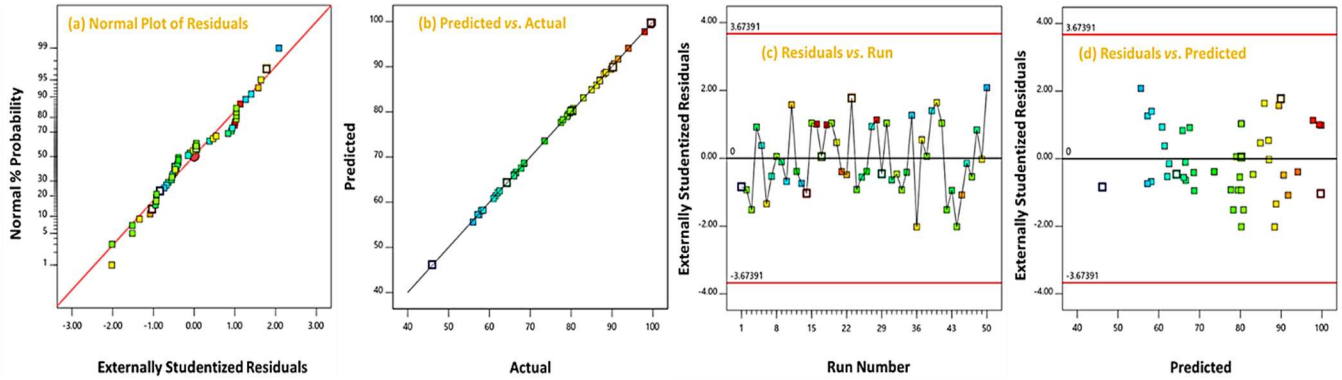

Fig. 11. Graphical plots of the a) Normal % Probability *vs.* Externally Studentized Residuals b) Predicted *vs.* Actual c) Externally Studentized Residuals *vs.* run Number and d) Externally Studentized Residuals *vs.* predicted.

Another parameter that can affect the loading of phenobarbital drugs on Ag/ZnO/SBA-16 nanocomposite is temperature. The process of drug loading on the nanocarrier was investigated at five temperatures of 30, 40, 50, 60, and 70 °C (Fig. 12d). The results showed that the amount of drug loading decreases with increasing temperature. This decrease in loading can be attributed to changes in Gibbs free energy. In the adsorption process, enthalpy changes are negative (exothermic) and entropy changes are positive. According to the equation of $\Delta G = \Delta H - T\Delta S$, with the decrease in temperature, Gibbs free energy becomes negative and the absorption process becomes spontaneous [58].

The contact time to achieve stable absorption is directly proportional to the drug loading capacity (Fig. 12e). The results showed that up to ~13 min, a rapid increase in loading occurs, which is due to an increase in the surface area of mesoporous silica particles ready for loading. In other words, in the first minutes, a large number of active sites of the nanocomposite are available to the drug molecules, therefore, the drug loading increases [59].

In Table 6, the optimal value of parameters affecting the amount of phenobarbital loading on Ag/ZnO/SBA-16 nanocomposite is shown. It also shows the predicted and experimental value of EE percentage in the drug loading process. The small difference between the predicted and experimental values ($\Delta EE\% = 0.28$) indicates the success of drug loading on the nanocarrier.

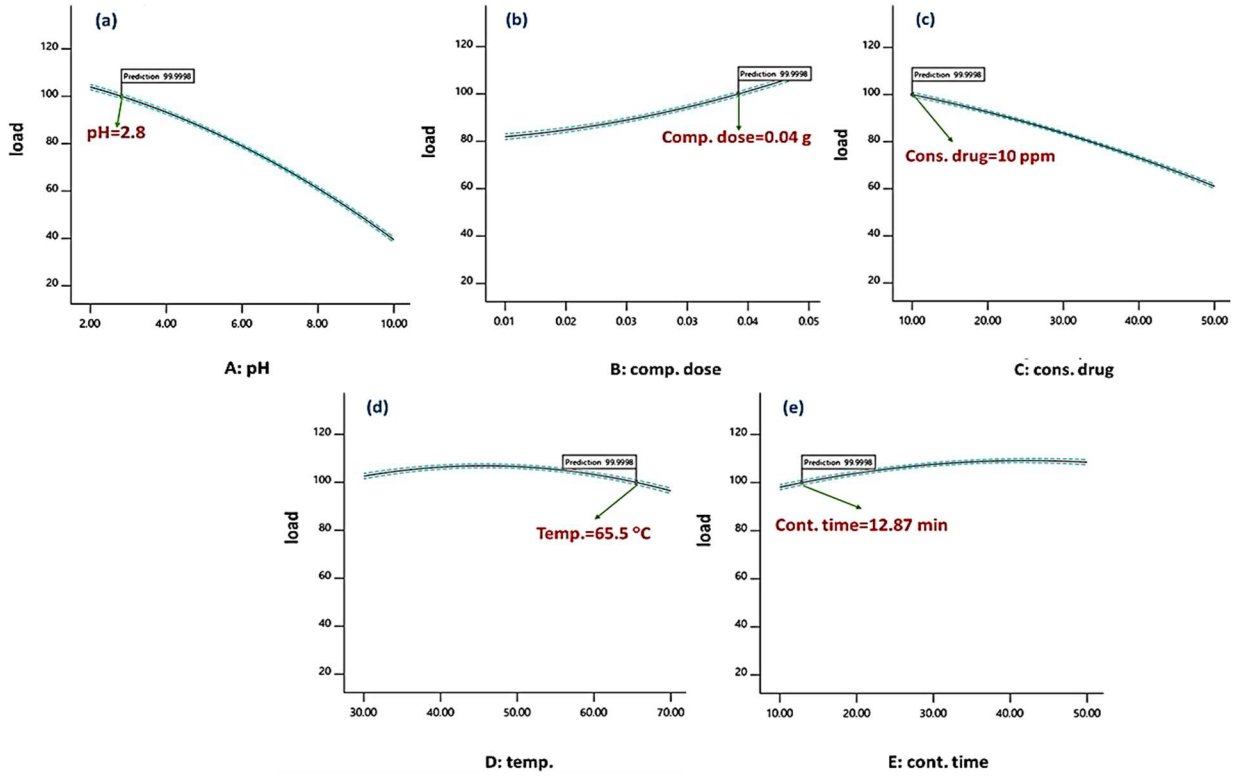

Fig. 12. The effect of main factors on the encapsulation EE% of Phenobarbital drug by Ag/ZnO/SBA-16 nanocomposite.

Table 6. Optimal Parameters and EE% for the Encapsulation of PHB Drug on Nanocarrier

pH	NCD	ICT	Temp.	CT	EE% (Predicted value)	EE% (Experimental value)	ΔEE%	Desirability
2.82	0.04	10.00	65.5	12.87	100	99.73	0.28	1

In this research, six isotherms of Langmuir, Freundlich, Temkin, Jovanovich, Redlich-Peterson, and Henry under optimal conditions were studied [60]. The calculated constants for all isotherms and their correlation coefficients (R^2) were calculated at the optimum temperature (Table 7 and Fig. 13). The results show that the correlation coefficients for the Freundlich model is 0.9966 and Redlich-Peterson are 0.9949, which is more suitable than the other models, which indicates the homogeneity of the absorbent structure [61].

Table 7. Isotherms Parameters for PHB Loading onto Ag/ZnO/SBA-16

50 ppm	40 ppm	30 ppm	20 ppm	10 ppm	Parameters	Model
14.0	9.9	4.6	1.8	0.3	C_e (ppm)	
27.00	22.57	19.05	13.65	7.27	q_e	Langmuir
0.037	0.044	0.050	0.070	0.137	$1/q_e$	
0.07	0.10	0.20	0.55	3.30	$1/C_e$	
	R^2 = 0.9702	K_L = 0.66 l mg^{-1}		q_{max}= 34.96		
14.0	9.9	4.6	1.8	0.3	C_e (ppm)	
27.00	22.57	19.05	13.65	7.27	q_e	Freundlich
1.43	1.35	1.27	1.13	0.86	$\log q_e$	
1.14	0.99	0.66	0.25	-0.52	$\log C_e$	
	R^2 = 0.9966	K_f = 10.95 (mg g^{-1}) (l mg^{-1})n		n = 2.98		
14.0	9.9	4.6	1.8	0.3	C_e (ppm)	
27.00	22.57	19.05	13.65	7.27	q_e	Temkin
3.29	3.11	2.94	2.61	1.10	$\ln q_e$	
2.63	2.30	1.52	0.58	-1.20	$\ln C_e$	
	R^2 = 0.9366	K_T = 1.26		B = 0.5531		
14.0	9.9	4.6	1.8	0.3	C_e (ppm)	
27.00	22.57	19.05	13.65	7.27	q_e	Jovanovich
3.29	3.11	2.94	2.61	1.98	$\ln q_e$	
	R^2 = 0.7771	K_J = 0.0794 l mg^{-1}		q_{max}= 9.97		
14.0	9.9	4.6	1.8	0.3	C_e (ppm)	
27.00	22.57	19.05	13.65	7.27	q_e	Redlich-Peterson
2.63	2.29	1.52	0.33	-1.20	$\ln C_e$	
-0.65	-0.82	-1.42	-2.02	-3.19	$\ln C_e/q_e$	
	R^2 = 0.9949	g = 0.656		a_g = 10.49		
14.0	9.9	4.6	1.8	0.3	C_e (ppm)	
27.00	22.57	19.05	13.65	7.27	q_e	Henry
	R^2 = 0.9058	K_{HE} = 1.279				

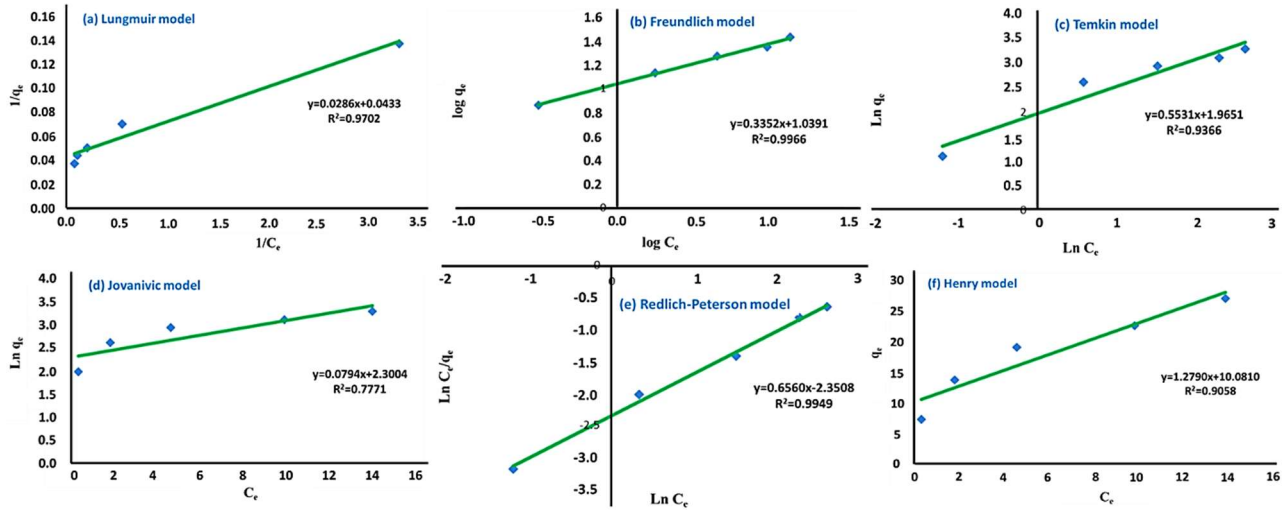

Fig. 13. Isotherms plots of (a) Langmuir, (b) Freundlich, (c) Temkin, (d) Jovanovich, (e) Redlich-Peterson, and (f) Henry for PHB adsorption.

The values of q_e and C_e were measured to calculate the thermodynamic functions of PHB drug loading on Ag/ZnO/SBA-16 nanocomposite at three temperatures of 303, 313, 323, 33, and 343 K under optimal conditions. Using the following equations, the values of thermodynamic functions were calculated [62]:

$$\ln K_c = -\frac{\Delta H^\circ}{RT} + \frac{\Delta S^\circ}{R} \quad (4)$$

$$\Delta G^\circ = -RT\ln K_c \quad (5)$$

$$\Delta G^\circ = \Delta H^\circ - T\Delta S^\circ \quad (6)$$

$$K_c = \frac{q_e}{C_e} \quad (7)$$

Where, ΔH°, ΔS°, ΔG°, and K_c are the standard enthalpy, entropy, Gibbs free energy, and equilibrium, respectively. According to the value of ΔH°, the absorption between the drug and nanocarrier is physical absorption. Also, the values of ΔG° show that the process of drug absorption on the drug carrier is spontaneous at low temperatures. The results are shown in Fig. 14 and Table 8.

To obtain the best kinetic model for PHB drug loading on Ag/ZnO/SBA-16 nanocarrier, seven zero-order (ZO), pseudo-first-order (PFO), pseudo-second-order (PSO), Higuchi model (HIG), Elovich (EL), and Avrami (AV) models using The following equations were investigated (Fig. 15 and Table 9) [63].

$$\text{ZO model:} \quad q_t = k_0 t + q_0 \quad (7)$$

$$\text{PFO model:} \quad \ln(q_e - q_t) = -k_1 t + \ln q_e \quad (8)$$

$$\text{PSO model:} \quad \frac{t}{q_t} = \frac{1}{q_e} t + \frac{1}{k_2 q_e^2} \quad (9)$$

$$\text{HIG model:} \quad q_t = k_i \sqrt{t} + C \quad (10)$$

$$\text{EL model:} \quad q_t = \beta \ln(\alpha\beta) - \ln t \quad (11)$$

$$\text{Av model:} \quad \ln(-\ln(1 - Q_t)) - q_t = -K_{av} + n_{av} \ln t \quad (12)$$

Table 8. Thermodynamic Parameters for the Adsorption of PHB Drug onto Ag/ZnO/SBA-16 at Different Temperatures

Temp. (K)	lnK$_c$	ΔH° (Kj mol^{-1})	ΔS° (Kj mol^{-1})	ΔG° (Kj mol^{-1})	R^2
303	4.45			-11.24	
313	3.91			-10.86	
323	3.88	-22.85	-0.038	-10.47	0.9999
333	3.63			-10.09	
343	3.35			-9.71	

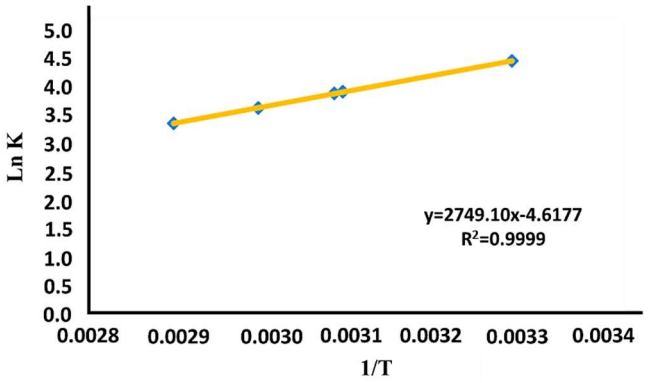

Fig. 14. lnK *vs.* 1/T for the adsorption of PHB drug onto Ag/ZnO/SBA-16.

According to the regression coefficient (R^2 = 0.9983), it can be concluded that the loading process of PHB drug on Ag/ZnO/SBA-16 nanocomposite corresponds to the Higuchi model (HIG) kinetic model (R^2 = 0.9983).

Figure 16 shows the graph of drug release experiments for three aqueous environments (green curve), an acidic environment (blue curve), and an alkaline environment (red curve). In 2011, Zeng *et al.* presented a theoretical kinetic model for drug release by silica nanoparticles [64]. In this model, it is assumed that drug release in the early hours has an explosive release and then it is a slow and stable release related to the release of drug molecules that are placed inside the pores of silica nanoparticles. The results of the study demonstrated fast release of drug from the nanoparticles in the initial 4 h, that is, 10% of the total drug was released in 4 h. The fast drug release from nanoparticles may be ascribed to the surface-loading (adsorption) of the drug at the particle

surface. The initial fast release of drug from nanoparticles may be ascribed to the fact that the drug is present on the surface of the nanoparticles. Drug molecules absorbed at the surface of the nanoparticles are released faster as compared to embedded drug. However, further drug release was found to be sustained [65].

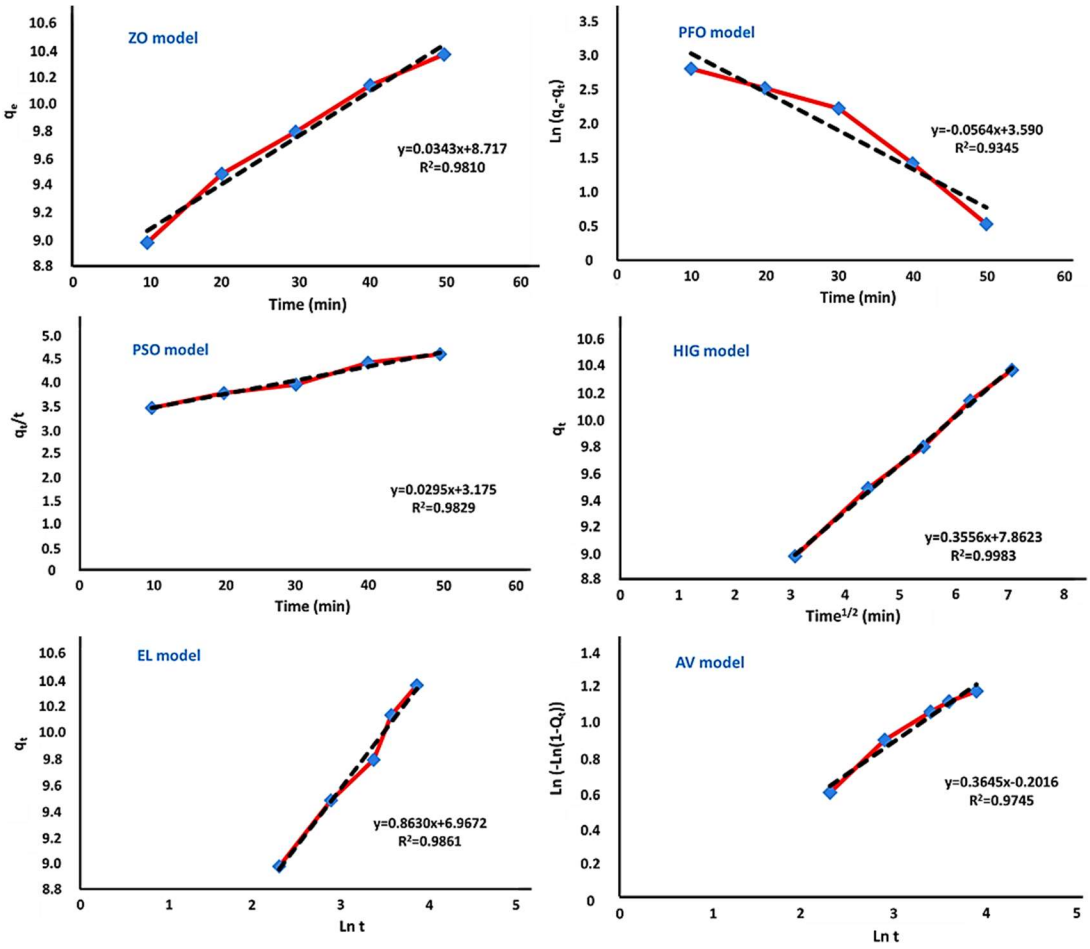

Fig. 15. Linear plots of kinetic models for loading of PHB onto Ag/ZnO/SBA-16.

Table 9. Kinetic Parameters were Obtained from the ZO, PFO, PSO, HIG, EL, and AV Models for the PHB Loading onto Ag/ZnO/SBA-16

Zero order model (ZO)			Pseudo-first-order model (PFO)		
k_0 (mol l^{-1} min^{-1})	q_e (mg g^{-1})	R^2	k_1 (min^{-1})	q_e (mg g^{-1})	R^2
0.0343	8.817	0.9810	-0.0564	1.25	0.9345
Pseudo-second-order model (PSO)			Higuchi model (HIG)		
k_2 (mol^{-1} l min^{-1})	q_e (mg g^{-1})	R^2	k_i (min^{-1})	R^2	
0.0003	33.89	0.9829	0.3556	0.9983	
Elovich model (EL)			Avrami model (AV)		
α (mg g^{-1} min^{-1})	β (g mg^{-1})	R^2	k_{av}	n_{av}	R^2
6.97	1.46	0.9861	1.22	0.3645	0.9745

Ag particles have excellent bioactivities against diverse species of microorganisms due to Ag ion release [66]. Indeed, Ag ion has a strong antibacterial property due to its multifunctional attack on sensitive and resistant microorganisms [67]. However, aggregation of Ag ions due to their oxidation leads to the loss of their bioactivities [68,69]. For this occurrence, the usage of an appropriate substrate can be effective solution to prevent prolonged bioactivities. For this purpose, the substrate should protect Ag nanoparticles to prevent ion immediate release. Ag/SBA-16 is known as a perfect substrate to load and carry Ag nanoparticles for a long period due to its controlled ion release [70,71]. However, it is expected that Ag/SBA-16 can save bioactivities due to its higher loaded Ag and more complex pore structure [72,73]. SBA-16 has no bioactivities due to its biodegradable nature. Also, their porosity can help to extend easier microorganisms. Hence, it is expected to not observe any antibacterial properties in all steps. According to high-loaded Ag nanoparticles in Ag/SBA-16 and their controlled release with appropriate dose, it is expected that they show prolonged and efficient bioactivities. This feature continues until the existence of enough ion dose in bulk tubes [74].

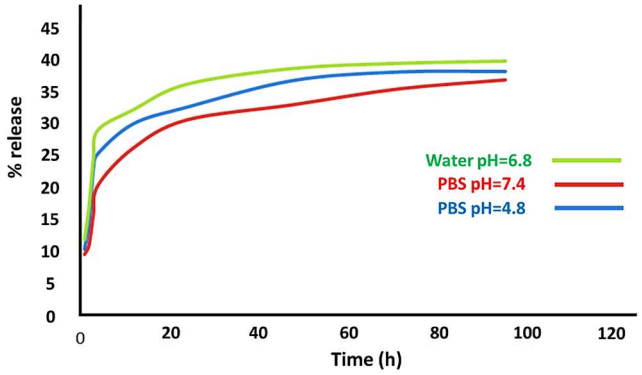

Fig. 16. *In vitro* release of PHB by Ag/ZnO/SBA-16 nanocomposite.

Also, to obtain the best kinetic model for PHB drug release four zero-order (ZO), pseudo-first-order (PFO), pseudo-second-order (PSO), and Higuchi model (HIG) models for three aqueous, acidic, and alkaline environments were studied (Fig. 17). The results show that drug release follows the Higuchi kinetic model (R^2 = 0.9969, 0.9991, and 0.9992 for aqueous, acidic, and alkaline environments, respectively) as well as drug loading.

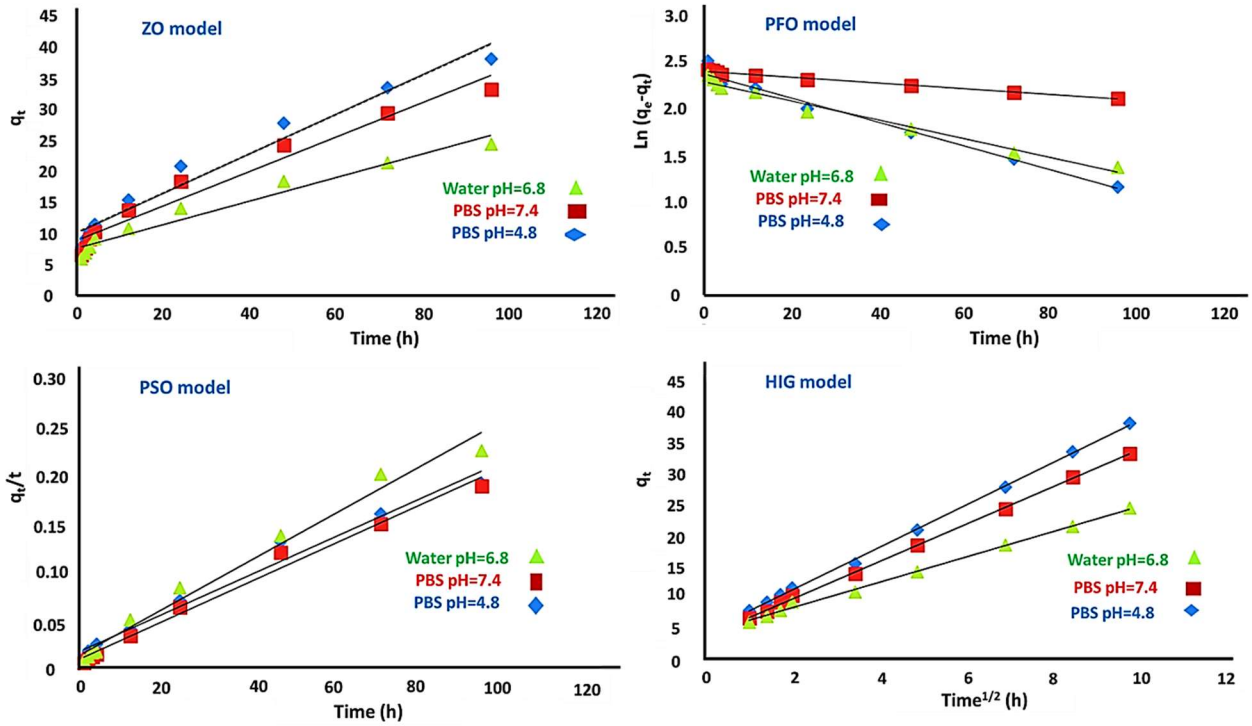

Fig. 17. Linear plots of kinetic models for release of PHB onto Ag/ZnO/SBA-16.

CONCLUSION

In this work, the Ag/ZnO/SBA-16 was synthesized and used as loading and release of phenobarbital drug. To identify and characterize the properties of Ag/ZnO/SBA-16 nanostructure, several identification methods such as XRD, FTIR, BET, EDX, SEM, and TEM were used. The influence of various parameters including pH, drug concentration, nanocomposite dose, temperature, and contact time was studied by RSM method. Drug release in three different environments at 37 ℃ including aqueous medium with pH = 6.8, acidic with pH = 4.8, and alkaline with pH = 7.4 at times of 1, 2, 3, 4, 12, 24, 48, 72, and 96 hours was studied. The data obtained from isotherm determination studies and drug loading kinetics showed that the drug loading process follows the Freundlich isotherm with R^2 = 0.9966 and the Higuchi kinetics model with R^2 = 0.9983. The thermodynamic study also showed that drug loading on Ag/ZnO/SBA-16 nanocomposite is an exothermic and spontaneous process at low temperatures.

REFERENCES

[1] Taylor, K. M.; Kim, J. S.; Rieter, W. J.; An, H.; Lin, W.; Lin, W., Mesoporous Silica Nanospheres as Highly Efficient MRI Contrast Agents. *J. Am. Chem. Soc*. **2008**, *130*, 2154. https://doi.org/10.1021/ja710193c.

[2] Shin, Y.; Chang, J. H.; Liu, J. R.; Williford, R.; Shin, Y. K.; Exarhos, G. J., Hybrid nanogels for sustainable positive thermosensitive drug release. *J. Controlled Release,* **2001**, *73*, 1. DOI: 10.1016/s0168-3659(01)00247-4.

[3] Han, Y. J.; Yu, Z. T.; Zhou, L., Hydroxyapatite/titania composite bioactivity coating processed by the sol-gel method. *Biomed. Mate.* **2008**, *3*, 044109, DOI: 10.1088/1748-6041/3/4/044109.

[4] Vallet-Reg, M.; Gonzalez-Calbet, J. M., Calcium Phosphates as Substitution of Bone Tissues. *Prog. Solid State Chem*. **2004**, *32*, 1. http://dx.doi.org/10.1016/j.progsolidstchem.2004.07.001

[5] Talib, M.; Abd Alkadir, A., Synthesis and characterization of mesoporous materials as a carrier and release of prednisolone in drug delivery system. *Journal of Drug Delivery Sci. Technol.* **2019**, *53*, 101176. https://doi.org/10.1016/j.jddst.2019.101176.

[6] Morales, V.; Martin, A.; Ortiz-Bustos, J.; Sanz, R., Effect of the dual incorporation of fullerene and polyethyleneimine moieties into SBA-15 materials as platforms for drug delivery. *J. Mater. Sci.* **2019**, *54*, 11635. DOI: 10.1007/s10853-019-03708-0.

[7] Trzeciak, K.; Chotera-Ouda, A.; Bak-Sypien, I. I.; Potrzebowski, M. J., Mesoporous Silica Particles as Drug Delivery Systems-The State of the Art in Loading Methods and the Recent Progress in Analytical Techniques for Monitoring These Processes. *Pharmaceutics*. **2021**, *13*, 950. DOI: 10.3390/ pharmaceutics13070950.

[8] Fekri, M. H.; Soleymani, S.; Razavi Mehr, M.; Akbari-adergani, B., Synthesis and characterization of mesoporous ZnO/SBA-16 nanocomposite: Its efficiency as drug delivery system. *J. Non-Cryst. Solids*. **2022**, *591*, 121512. https://doi.org/10.1016/j.jnoncrysol. 2022.121512.

[9] Prabha, S.; Durgalakshmi, D.; Rajendran, S.; Lichtfouse, E., Plant-derived silica nanoparticles and composites for biosensors, bioimaging, drug delivery and supercapacitors: a review. *Environmental Chemistry Letters*. **2021**, *19*, 1667-1691. https://doi.org/10.1007/s10311-020-01123-5

[10] Wang, S., Ordered mesoporous materials for drug delivery. *Microporous Mesoporous Mater.* **2009**, *117*, 1. https://doi.org/10.1016/j.micromeso.2008.07.002.

[11] Morey, M.; Davidson, A.; Eckert, H.; Stucky, G., Silica-Based, Cubic Mesostructures: Synthesis, Characterization and Relevance for Catalysis. *Chem. Mater*. **1996**, *8*, 486. https://doi.org/10.1021/cm950397j.

[12] Yu, B.; Shi, R.; Chen, X.; Zhang, Y.; Hu, J.; Khan, S., Gelatin-coated indomethacin drug-loaded SBA-16 silica-based composites: pH-responsive slow-release performance. *Inorganic Chemistry Communications*. **2023**, *150*, 110469. https://doi.org/10.1016/j.inoche.2023.110469.

[13] Costa, J. A. S.; de Jesus, R. A.; Santos, D. O.; Neris, J. B.; Figueiredo, R. T.; Paranhos, C. M., Synthesis, functionalization, and environmental application of silica-based mesoporous materials of the M41S and SBA-n families: A review. *Journal of Environmental Chemical Engineering*, **2021**, *9*, 105259.

https://doi.org/10.1016/j.jece.2021.105259.

[14] Ezzeddine, Z.; Batonneau-Gener, I.; Pouilloux, Y., Zinc Removal from Water *via* EDTA-Modified Mesoporous SBA-16 and SBA-15. *Toxics*, **2023**, *11*, 205. https://doi.org/10.3390/toxics11030205.

[15] Wang, X.; Jia, J.; Zhao, L.; Sun, T., Chemisorption of hydrogen sulphide on zinc oxide modified aluminum-substituted SBA-15. *Appl. Surf. Sci.* **2008**, *254*, 5445. https://doi.org/10.1016/j.apsusc.2008.02.086.

[16] Hu, Y.; Zhi, Z.; Zhao, Q.; Wua, C.; Zhao, P.; Jiang, H.; Jiang, T.; Wang, S., 3D cubic mesoporous silica microsphere as a carrier for poorly soluble drug carvedilol. *Microporous Mesoporous Mater.* **2012**, *147*, 94. DOI: 10.1016/j.micromeso.2011.06.001.

[17] Akintelu, S. A.; Folorunso, A. S., A review on green synthesis of zinc oxide nanoparticles using plant extracts and its biomedical applications. *BioNanoScience*, **2020**, *10*, 848-863. https://doi.org/10.1007/s12668-020-00774-6.

[18] Mishra, P. K.; Mishra, H.; Ekielski, A.; Talegaonkar, S.; Vaidya, B., Zinc oxide nanoparticles: a promising nanomaterial for biomedical applications. *Drug Discovery Today*, **2017**, *22*, 1825-1834. https://doi.org/10.1016/j.drudis.2017.08.006.

[19] Zhang, Z. Y.; Xiong, H. M., Photoluminescent ZnO nanoparticles and their biological applications. *Materials*, **2015**, *8*, 3101-3127. https://doi.org/10.3390/ma8063101.

[20] Kim, S.; Lee, S. Y.; Cho, H. J., Doxorubicin-wrapped zinc oxide nanoclusters for the therapy of colorectal adenocarcinoma. *Nanomaterials*, **2017**, *7*, 354. https://doi.org/10.3390/nano7110354.

[21] Xiong, H. M., ZnO nanoparticles applied to bioimaging and drug delivery. *Advanced Materials*, **2013**, *25*, 5329-5335. https://doi.org/10.1002/adma.201301732.

[22] Wiesmann, N.; Tremel, W.; Brieger, J., Zinc oxide nanoparticles for therapeutic purposes in cancer medicine. *Journal of Materials Chemistry B*, **2020**, *8*, 4973-4989. https://doi.org/10.1039/D0TB00739K.

[23] Jayaseelan, C.; Rahuman, A. A.; Kirthi, A. V.; Marimuthu, S.; Santhoshkumar, T.; Bagavan, A.; ... & Rao, K., Novel microbial route to synthesize ZnO nanoparticles using Aeromonas hydrophila and their activity against pathogenic bacteria and fungi. *Spectrochimica Acta Part A: Molecular and Biomolecular Spectroscopy*, **2012**, *90*, 78-84. https://doi.org/10.1016/j.saa.2012.01.006.

[24] Baum, M. K.; Shor-Posner, G.; Campa, A., Zinc status in human immunodeficiency virus infection. *The Journal of Nutrition*, **2000**, *130*, 1421S-1423S. https://doi.org/10.1093/jn/130.5.1421S.

[25] Hiller, J. M.; Perlmutter, A., Effect of zinc on viral-host interactions in a rainbow trout cell line, RTG-2. *Water Research*, **1971**, *5*, 703-710. https://doi.org/10.1016/0043-1354(71)90092-3.

[26] Rasmussen, J. W.; Martinez, E.; Louka, P.; Wingett, D., Zinc oxide nanoparticles for selective destruction of tumor cells and potential for drug delivery applications. *Expert Opinion on Drug Delivery*, **2010**, *7*, 1063-1077. https://doi.org/10.1517/17425247.2010.502560.

[27] Nikolova, S.; Milusheva, M.; Gledacheva, V.; Feizi-Dehnayebi, M.; Kaynarova, L.; Georgieva, D.; ... & Todorova, M, Drug-delivery silver nanoparticles: A new perspective for phenindione as an anticoagulant. *Biomedicines*, **2023**, *11*, 2201. https://doi.org/10.3390/biomedicines11082201.

[28] Trinka, E., Phenobarbital in Status epilepticus-Rediscovery of an effective drug. *Epilepsy & Behavior*. **2023**, *141*, 109104. https://doi.org/10.1016/j.yebeh.2023.109104.

[29] Stöber, W.; Fink, A.; Bohn, E., Controlled growth of monodisperse silica spheres in the micron size range. *Journal of colloid and Interface Science*, **1968**, *26*, 62-69. https://doi.org/10.1016/0021-9797(68)90272-5.

[30] Sivakumar, M.; Sakthivel, M.; Chen, S. M., Activated carbon-ZnO nanocomposite for electrochemical sensing of acetaminophen. *International Journal of Electrochemical Science*, **2016**, *11*, 8363-8373. https://doi.org/10.20964/2016.10.51.

[31] Wen, H.; Zhou, X.; Shen, Z.; Peng, Z.; Chen, H.; Hao, L.; Zhou, H., Synthesis of ZnO nanoparticles supported on mesoporous SBA-15 with coordination effect-assist for anti-bacterial assessment. *Colloids and Surfaces B: Biointerfaces*, **2019**, *181*, 285-294. https://doi.org/10.1016/j.colsurfb.2019.05.055.

[32] Azizi, S. N.; Ghasemi, S.; Samadi-Maybodi, A.; Ranjbar-Azad, M., A new modified electrode based on

Ag-doped mesoporous SBA-16 nanoparticles as non-enzymatic sensor for hydrogen peroxide. *Sensors and Actuators B: Chemical*, **2015**, *216*, 271-278. https://doi.org/10.1016/j.snb.2015.03.078.

[33] Bakatula, E. N.; Richard, D.; Neculita, C. M.; Zagury, G. J., Determination of point of zero charge of natural organic materials. *Environ. Sci. Pollut. Res. Int.* **2018**, *25*, 7823. DOI: 10.1007/s11356-017-1115-7.

[34] Sarkar, S.; Tiwari, N.; Behera, M.; Chakrabortty, S.; Jhingran, K.; Sanjay, K.; ... & Tripathy, S. K., Facile synthesis, characterization and application of magnetic Fe_3O_4-coir pith composites for the removal of methyl violet from aqueous solution: Kinetics, isotherm, thermodynamics and parametric optimization. *Journal of the Indian Chemical Society*, **2022**, *99*, 100447. https://doi.org/10.1016/j.jics.2022.100447.

[35] Fekri, M. H.; Shahverdi, V.; Chegeni, M.; Razavi Mehr, M., Abbastabar Ahangar, H.; Saffar, A., Simultaneous photocatalytic degradation of cefixime and cefuroxime antibiotics using g-C_3N_4/$NaBiO_3$ nanocomposite and optimization of effective parameters by response surface methodology. *Reaction Kinetics, Mechanisms and Catalysis*. **2022**, *135*, 1059. https://doi.org/10.1007/s11144-022-02192-z.

[36] Reji, M.; Kumar, R., Response surface methodology (RSM): An overview to analyze multivariate data. *Indian J. Microbiol. Res.*, **2022**, *9*, 241-248. https://doi.org/10.18231/j.ijmr.2022.042.

[37] Poonia, E.; Duhan, S.; Kumar, K.; Kumar, A.; Jakhar, S.; Tomer, V. K., One pot hydrothermal synthesis of ordered mesoporous SnO_2/SBA-16 nanocomposites. *J. Porous Mater.* **2019**, *26*, 1. DOI: 10.1007/s10934-018-0651-y.

[38] Zhang, X.; Qu, Z., Li, X.; Zhao, Q.; Zhang, X.; Quan, X., In-situ synthesis of Ag/SBA-15 nanocomposites by the "pH-adjusting" method. *Mater. Lett.* **2011**, *65*, 1892. https://doi.org/10.1016/j.matlet.2011.03.072.

[39] El-Nahhal, I. M.; Salem, J. K.; Al-agha, A., Silver-NPs functionalized hexagonal SBA-15 and lamellar SiO_2-L81 mesoporous silica, synthesis and structural characterization. *J. Sol-Gel Sci. Technol.* **2020**, *93*, 175. DOI: https://doi.org/10.1007/s10971-019-05128-7.

[40] Gupta, R.; Layek, S.; Pathak, D. D., Synthesis and characterization of guanine-functionalized mesoporous silica [SBA-16-G]: a metal-free and recyclable heterogeneous solid base catalyst for synthesis of pyran-annulated heterocyclic compounds, *Research on Chemical Intermediates* **2019**, *45*, 1619-1637. DOI: 10.1007/s11164-018-3693-5.

[41] Khanh Nguyen, Q. N.; Yen, N. T.; Hau, N. D.; Tran, H. L., Synthesis and Characterization of Mesoporous Silica SBA-15 and ZnO/SBA-15 Photocatalytic Materials from the Ash of Brickyards. *Journal of Chemistry*, **2020**, *2020*, https://doi.org/10.1155/2020/8456194).

[42] Zhou, Y., Synthesis, characterization, and photo-catalytic activity of Ag/ZnO/SBA-15 composite. *Desalination and Water Treatment*, **2019**, *159*, 250-256. https://doi:10.5004/dwt.2019.24116.

[43] Pourdayhimi, P.; Koh, P. W.; Salleh, M. M.; Nur, H.; Lee, S. L., Zinc oxide nanoparticles-immobilized mesoporous hollow silica spheres for photodegradation of sodium dodecylbenzenesulfonate. *Australian Journal of Chemistry*, **2016**, *69*, 790-797. https://doi.org/10.1071/CH15495.

[44] Budi, C. S.; Deka, J. R.; Saikia, D.; Kao, H. M.; Yang, Y. C., Ultrafine bimetallic Ag-doped Ni nanoparticles embedded in cage-type mesoporous silica SBA-16 as superior catalysts for conversion of toxic nitroaromatic compounds. *Journal of Hazardous Materials*, **2020**, *384*, 121270. https://doi.org/10.1016/j.jhazmat.2019.121270.

[45] Zhao, D.; Huo, Q.; Feng, J.; Chmelka, B. F.; Stucky, G. D., Nonionic Triblock and Star Diblock Copolymer and Oligomeric Surfactant Syntheses of Highly Ordered, Hydrothermally Stable, Mesoporous Silica Structures. *J. Am. Chem. Soc.* **1998**, *120*, 6024. https://doi.org/10.1021/ja974025i.

[46] Kim, T. W.; Ryoo, R.; Gierszal, K. P.; Jaroniec, M.; Solovyov, L. A.; Sakamoto, Y.; Terasaki, O., Characterization of mesoporous carbons synthesized with SBA-16 silica template. *Journal of Materials Chemistry*, **2005**, *15*, 1560-1571. https://doi.org/10.1039/B417804A.

[47] Wang, X.; Mei, J.; Zhao, Z.; Chen, Z.; Zheng, P.; Fu, J.; Li, H.; Fan, J.; Duan, A.; Xu, C., Controllable Synthesis of Spherical Al-SBA-16 Mesoporous Materials with Different Crystal Sizes and Its High Isomerization Performance for Hydrodesulfurization of Dibenzothiophene and 4,6-Dimethyldibenzothiophene.

Ind. Eng. Chem. Res. **2018**, *57*, 2498. https://doi.org/10.1021/acs.iecr.8b00109.

[48] Banafti, S.; Jahanshahi, M.; Peyravi, M.; Khalili, S., Controllable release activity of antibacterial Ag/SBA-16 cage-like synthesized by one-pot method. *Microporous and Mesoporous Mater*. **2020**, *299*, 110107. https://doi.org/10.1016/j.micromeso.2020.110107.

[49] Dalvand, A.; Nabizadeh, R.; Ganjali, M. R.; Khoobi, M.; Nazmara, S.; Mahvi, A. H., Modeling of Reactive Blue 19 azo dye removal from colored textile wastewater using L-arginine-functionalized Fe_3O_4 nanoparticles: Optimization, reusability, kinetic and equilibrium studies. *Journal of Magnetism and Magnetic Materials*, **2016**, *404*, 179-189. https://doi.org/10.1016/j.jmmm.2015.12.040.

[50] Reghioua, A.; Barkat, D.; Jawad, A. H.; Abdulhameed, A. S.; Al-Kahtani, A. A.; ALOthman, Z. A., Parametric optimization by Box-Behnken design for synthesis of magnetic chitosan-benzil/ZnO/Fe_3O_4 nanocomposite and textile dye removal. *Journal of Environmental Chemical Engineering*, **2021**, *9*, 105166. https://doi.org/10.1016/j.jece.2021.105166.

[51] Kang, J. K.; Kim, Y. G.; Lee, S. C.; Jang, H. Y.; Yoo, S. H.; Kim, S. B., Artificial neural network and response surface methodology modeling for diclofenac removal by quaternized mesoporous silica SBA-15 in aqueous solutions. *Microporous and Mesoporous Materials*, **2021**, *328*, 111497. https://doi.org/10.1016/j.micromeso.2021.111497.

[52] Jaswir, I.; Noviendri, D.; Taher, M.; Mohamed, F.; Octavianti, F.; Lestari, W.; ... & Hamad Almansori, B. B., Optimization and formulation of fucoxanthin-loaded microsphere (F-LM) using response surface methodology (RSM) and analysis of its fucoxanthin release profile. *Molecules*, **2019**, *24*, 947. https://doi.org/10.3390/molecules24050947.

[53] Zhang, X.; Zhou, J.; Xu, Y., Optimized parameters for the preparation of silk fibroin drug-loaded microspheres based on the response surface method and a genetic algorithm-backpropagation neural network model. *Journal of Biomedical Materials Research Part B: Applied Biomaterials*, **2021**, *109*, 6-18. https://doi.org/10.1002/jbm.b.34676.

[54] Mohammed, B. B.; Hsini, A.; Abdellaoui, Y.; Abou Oualid, H.; Laabd, M.; El Ouardi, M.; ... & Tijani, N., Fe-ZSM-5 zeolite for efficient removal of basic Fuchsin dye from aqueous solutions: Synthesis, characterization and adsorption process optimization using BBD-RSM modeling. *Journal of Environmental Chemical Engineering*, **2020**, *8*, 104419. https://doi.org/10.1016/j.jece.2020.104419.

[55] Afrashteh, S.; Nouri, N.; Banihashem, P.; Hoseinpour Kasgari, A.; Valipour, P.; Binaeian, E., Methotrexate drug uptake through dimethyl ethylenediamine post-modified metal-organic framework as a carrier: optimization using RSM. *Journal of Porous Materials*, **2023**, *30*, 1625-1641. https://doi.org/10.1007/s10934-023-01441-3.

[56] Soleymani, S.; Razavi Mehr, M.; Fekri, M. H.; Saki, F., Modification of SBA-16 surface by-NH_2 group and its application as adsorbent. *Chemical Papers*, **2023**, *77*, 5129-5141. https://doi.org/10.1007/s11696-023-02849-6.

[57] Fekri, M. H.; Saki, F.; Razavi-mehr, M.; Soleymani, S., Preparation of SBA-16 silicate nanoabsorbent by green method from reed plant stem, using it to remove Phenolphthalein pollutant and investigating effective factors by RSM method. *Applied Chemistry*, **2023**, *18*, 271-288. https://doi.org/10.22075/chem.2023.29594.2141.

[58] Fekri, M. H.; Mohamareh, S. I.; Hosseini, M.; Mehr, M. R., Green synthesis of activated carbon/Fe_3O_4 nanocomposite from flaxseed and its application as adsorbent and antibacterial agent. *Chemical Papers*, **2022**, *76*, 6767-6782. https://doi.org/10.1007/s11696-022-02278-x.

[59] Fard, N. T.; Panahi, H. A.; Banadaki, M. D.; Moniri, E.; Soltani, E. R., Surface modification of graphene oxide by functionalized dendritic polyesters based on phthalic acid and pentaerythritol as a novel nanoplatform for sustained drug delivery: Statistical optimization using response surface methodology and release kinetics modelling. *Materials Today Communications*, **2023**, *36*, 106476. https://doi.org/10.1016/j.mtcomm.2023.106476.

[60] Albayati, T. M.; Salih, I. K.; Alazzawi, H. F., Synthesis and characterization of a modified surface of SBA-15 mesoporous silica for a chloramphenicol drug delivery system. *Heliyon*. **2019**, *5*, e02539.

https://doi.org/10.1016/j.heliyon.2019.e02539.

[61] Belhachemi, M.; Addoun, F., Comparative adsorption isotherms and modeling of methylene blue onto activated carbons. *Appl. Water Sci.* **2011**, *1*, 111. https://doi.org/10.1007/s13201-011-0014-1.

[62] Fekri, M. H.; Banimahd Keivani, M.; Razavi Mehr, M.; Akbari-adergani, B., Effective Parameters on Removal of Rhodamine B from Colored Wastewater by Nano polyaniline/Sawdust Composite. *Journal of Mazandaran University of Medical Sciences*, **2019**, *29*.

[63] Benjelloun, M.; Miyah, Y.; Akdemir Evrendilek, G.; Zerrouq, F.; Lairini, S., Recent Advances in Adsorption Kinetic Models: Their Application to Dye Types. *Arabian J. Chem*. **2021**, *14*, 103031. DOI: 10.1016/j.arabjc.2021.103031.

[64] Zeng, L.; An, L.; Wu, X., Modeling Drug-Carrier Interaction in the Drug Release from Nanocarrier. *Drug Delivery*. **2011**, *2011*. https://doi.org/10.1155/2011/370308.

[65] Sharma, H.; Kumar, K.; Choudhary, C.; Mishra, P. K.; Vaidya, B., Development and characterization of metal oxide nanoparticles for the delivery of anticancer drug. *Artificial Cells, Nanomedicine, and Biotechnology*, **2016**, *44*, 672-679. https://doi.org/10.3109/21691401.2014.978980.

[66] Ghandour, W.; Hubbard, J. A.; Deistung, J.; Hughes, M. N.; Poole, R. K., The uptake of silver ions by Escherichia coli K12: toxic effects and interaction with copper ions. *Applied Microbiology and Biotechnology*, **1988**, *28*, 559-565. https://doi.org/10.1007/BF00250412.

[67] Jones, S. A.; Bowler, P. G.; Walker, M.; Parsons, D., Controlling wound bioburden with a novel silver-containing Hydrofiber® dressing. *Wound Repair and Regeneration*, **2004**, *12*, 288-294. https://doi.org/10.1111/j.1067-1927.2004.012304.x.

[68] Lok, C. N.; Ho, C. M.; Chen, R.; He, Q. Y.; Yu, W. Y.; Sun, H.; ... & Che, C. M., Silver nanoparticles: partial oxidation and antibacterial activities. *JBIC Journal of Biological Inorganic Chemistry*, **2007**, *12*, 527-534. https://doi.org/10.1007/s00775-007-0208-z.

[69] Pal, S.; Tak, Y. K.; Song, J. M., Does the antibacterial activity of silver nanoparticles depend on the shape of the nanoparticle? A study of the gram-negative bacterium Escherichia coli. *Applied and Environmental Microbiology*, **2007**, *73*, 1712-1720. https://doi.org/10.1128/AEM.02218-06.

[70] Zhang, X.; Qu, Z.; Li, X.; Zhao, Q.; Zhang, X.; Quan, X., *In-situ* synthesis of Ag/SBA-15 nanocomposites by the "pH-adjusting" method. *Materials Letters*, **2011**, *65*, 1892-1895. https://doi.org/10.1016/j.matlet.2011.03.072.

[71] Tian, D.; Yong, G.; Dai, Y.; Yan, X.; Liu, S., CO oxidation catalyzed by Ag/SBA-15 catalysts prepared *via in situ* reduction: the influence of reducing agents. *Catalysis Letters*, **2009**, *130*, 211-216. https://doi.org/10.1007/s10562-009-9865-6.

[72] Ouargli, R.; Hamacha, R.; Benharrats, N.; Boos, A.; Bengueddach, A., β-diketone functionalized SBA-15 and SBA-16 for rapid liquid-solid extraction of copper. *Journal of Porous Materials*, **2015**, *22*, 511-520. https://doi.org/10.1007/s10934-015-9921-0.

[73] Kim, T. W.; Ryoo, R.; Kruk, M.; Gierszal, K. P.; Jaroniec, M.; Kamiya, S.; Terasaki, O., Tailoring the pore structure of SBA-16 silica molecular sieve through the use of copolymer blends and control of synthesis temperature and time. *The Journal of Physical Chemistry B*, **2004**, *108*, 11480-11489. https://doi.org/10.1021/jp048582k.

[74] de Oliveira Lima, A. M.; Fragal, E. H.; Caldas, B. S.; Nakamura, T. U.; Rubira, A. F.; Silva, R., Functional mesoporous silica decorated with Ag nanoparticles as chemo-photothermal agents. *Microporous and Mesoporous Materials*, **2022**, *341*, 112097. https://doi.org/10.1016/j.micromeso.2022.112097.